Journal of Fluids and Structures 17 (2003) 629–642

JOURNAL OF FLUIDS AND STRUCTURES

www.elsevier.nl/locate/jnlabr/yjfls

On the infrasound generated when a train enters a tunnel

M.S. Howe*

College of Engineering, Boston University, 110 Cummington Street, Boston, MA 02215, USA

Received 24 September 2001; accepted 4 December 2002

Abstract

An analysis is made of the 'open air infrasound' generated when a train enters a tunnel. For a tunnel of nominal radius R and train speed U the acoustic frequency $\sim U/R$ and wavelength $\sim R/M \gg R$, where M is the train Mach number. Infrasound is inaudible, but the pressure fluctuations generated by a high-speed train ($M > 0.2$) can cause annoying vibrations and 'rattles' in dwellings and other buildings close to a tunnel portal. Detailed calculations are presented in this paper for a 'hood-like' portal modelled analytically by the end of a circular cylindrical, thin-walled duct, and for an axisymmetric 'train' entering along the axis of the duct. A slender body approximation is used to model the influence of the moving train, and the acoustic problem is solved using the exact Green's function for a semi-infinite cylinder. Predictions are in good agreement with recent track-side measurements reported by Iida et al. (Proceedings of the 50th Japan National Congress on Theoretical and Applied Mechanics) for model scale experiments conducted at Mach numbers M as large as 0.33. However, both measurements and theory indicate that in applications at full scale it may be important to include in estimates of the infrasound the nonacoustic 'near-field' pressures produced by the passing train.

1. Introduction

A train entering a tunnel generates a compression wave that propagates ahead of the train, into the tunnel at the speed of sound (Hara et al., 1968; Fox and Vardy, 1973; Woods and Pope, 1976). In a long tunnel the compression wavefront can experience nonlinear steepening ultimately manifested by a loud, impulsive bang or 'crack' (called a 'micro-pressure' wave) radiating from the distant tunnel exit when the compression wave arrives (Ozawa et al., 1976, 1991; Ozawa Maeda, 1988). In addition, however, inaudible low-frequency pressure fluctuations (*infrasound* at frequencies $\sim$10–20 Hz) are also radiated from the vicinity of the tunnel portal into the open air when the train enters (and leaves) the tunnel (Iida et al., 2000, 2001). These waves can vibrate and 'rattle' structures in neighbouring buildings; they constitute a potentially important environmental hazard and a deterrent to the introduction of very high-speed operations (up to 500 kph) in urban areas.

Fig. 1 illustrates schematically the manner in which the ambient infrasound generated when a train enters a tunnel is studied by Iida et al. (2000, 2001) using model-scale experiments (for which the characteristic 'infrasound' frequency is about 2 kHz). An axisymmetric 'train' of total length ℓ consists of a circular cylindrical mid-section of radius h and cross-sectional area $\mathscr{A}_o = \pi h^2$, fitted with ellipsoidal nose and tail pieces each of length L. It is projected at speeds U up to 400 kph into a tunnel formed by a circular cylindrical, hard walled duct of radius R. The model train is guided by a tightly stretched steel wire extending along the centre-line of the tunnel and passing through a smooth cylindrical hole drilled along the train axis. The Reynolds number of the air flow induced by a train is large enough for the interaction between the train and tunnel portal to be regarded as inviscid (including the influence of the separated 'exit flow' from

*Corresponding author. Tel.: +1-617-484-0656; fax: +1-617-353-5866.
E-mail address: mshowe@bu.edu (M.S. Howe).

0889-9746/03/$ - see front matter
doi:10.1016/S0889-9746(03)00004-5

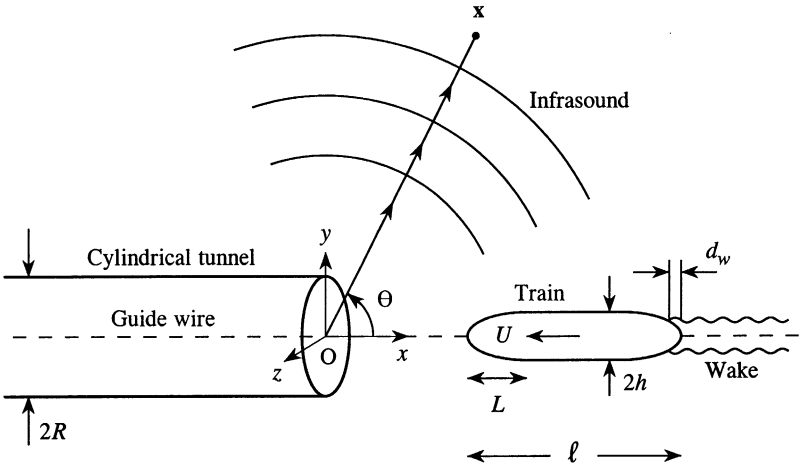

Fig. 1. Schematic model-scale experimental apparatus for studying the infrasound generated at a tunnel portal by an entering high-speed train.

the tunnel of the air displaced by the entering train). The properties of the sound produced by the interaction will therefore scale predominantly on train Mach number $M=U/c_o$ (c_o = speed of sound in air) and on the 'blockage' $\mathscr{A}_o/\mathscr{A}$, where $\mathscr{A}=\pi R^2$ is the cross-sectional area of the tunnel. Model scale experiments will accordingly supply a reliable indication of full scale results provided M and relative physical dimensions of the tunnel and train are the same (Ozawa et al., 1976; Ozawa and Maeda, 1988).

The purpose of this paper is to investigate the dependence of the infrasound on the train Mach number by exact analysis of a simple canonical problem. This will extend to arbitrary Mach number the approximate analyses of Iida et al. (2000, 2001) and of Howe (2001), who found that the infrasound amplitude varies as M^3 at small Mach numbers.

The canonical problem is motivated by the method used by the author (Howe, 1998a, b; 1999) for the compression wave problem, which was subsequently validated by model scale experiments (Howe et al., 2000). Introduce rectangular coordinates $\mathbf{x}=(x, y, z)$ with origin O on the axis of symmetry in the tunnel entrance plane of Fig. 1, with the negative x-axis coinciding with the axis of the tunnel. In the experiments the tunnel is sufficiently long that it may be regarded as extending to $x=-\infty$ for the purposes of calculation. The train nose profile is streamlined with aspect ratio $h/L\sim\frac{1}{3}$, and flow separation over the nose region will therefore be neglected. However, it will be necessary to include the influence of wake separation from the tail region of the train, as indicated in the figure. The train is assumed to enter the tunnel at constant speed U. In the envisaged applications the Mach number $M\leq 0.4$, and the blockage $\mathscr{A}_o/\mathscr{A}$ is usually less than about 0.2.

In the presence of the moving train the air pressure $\bar{p}$, density ρ, and sound speed c, become functions of position $\mathbf{x}$ and time t. Let their respective undisturbed values be denoted by p_o, ρ_o, c_o. Thermal and frictional losses occurring during the interaction of the train with the tunnel entrance will be ignored. The air flow may therefore be regarded as adiabatic and the infrasound calculated from the corresponding aeroacoustic equation for the production of sound in the presence of a moving surface (Howe, 1998a)

$$\left(\frac{\mathrm{D}}{\mathrm{D}t}\left(\frac{1}{c^2}\frac{\mathrm{D}}{\mathrm{D}t}\right)-\frac{1}{\rho}\boldsymbol{\nabla}\bullet(\rho\boldsymbol{\nabla})\right)B=\frac{1}{\rho}\mathrm{div}(\rho\boldsymbol{\omega}\boldsymbol{\nabla}\mathbf{v}), \tag{1.1}$$

where $\mathbf{v}(\mathbf{x}, t)$ is the velocity of the air $\boldsymbol{\omega}=curl\ \mathbf{v}$ is the vorticity, and $B=\int \mathrm{d}\bar{p}/\rho(\bar{p})+\frac{1}{2}v^2$ is the total enthalpy. The vorticity $\boldsymbol{\omega}$ is nonzero principally within the shear layers of the exit flow from the tunnel entrance of the air displaced by the advancing train and in the wake of the train; separation and vorticity production elsewhere on the train are ignored. In these circumstances B is constant throughout the fluid when the train is absent, and may therefore be assumed to vanish in the far field prior to the entry of the train into the tunnel. The air at large distances from the tunnel entrance is linearly perturbed from its undisturbed state, where we can take

$$B\approx\frac{p}{\rho_o},\quad p=\bar{p}-p_o. \tag{1.2}$$

The moving train is acoustically equivalent to a continuum of monopole and dipole sources distributed over the nose and tail regions where the cross-sectional area of the train is variable. The monopoles account for the displacement of

air ahead of and to the rear of the train. Pressure forces over the nose and tail produce a distributed drag force represented by the dipoles. Howe et al. (2000) obtained the following slender body approximation for the combined distributions of these monopoles and dipoles:

$$U\left(1+\frac{\mathscr{A}_o}{\mathscr{A}}\right)\frac{\partial}{\partial t}\left(\frac{\partial \mathscr{A}_T}{\partial x}(x+Ut)\delta(y)\delta(z)\right), \tag{1.3}$$

where $\mathscr{A}_T(s)$ is the cross-sectional area of the train at distance *s from the tip of the nose*, which is taken to cross the entrance plane of the tunnel at time $t=0$. The approximation replaces the exact monopole and dipole distributions on the surface of the train by a line source on those sections of the train axis where the cross-sectional area is variable, in the vicinities of the train nose and tail. The contribution of the term in $\mathscr{A}_o/\mathscr{A}$ in (1.3) represents the effect of the drag dipole. According to Howe et al. (2000) the slender body approximation is expected to be valid at least for $\mathscr{A}_o/\mathscr{A}\leq 0.2$, which covers most situations at full scale involving high-speed operations. This representation of the train has been found to yield excellent predictions of the compression wave generated when the front of the train enters the tunnel for several different tunnel portal geometries (Howe et al., 2000; Yoon and Lee, 2001).

In these calculations of the compression wave the train is usually assumed to be very long, and the tail and its wake are therefore ignored. To determine the infrasound, however, it is also be necessary to include the sound produced as the tail enters the tunnel. To do this the influence of the wake must be modelled; its contribution to the radiation is governed by the vortex source on the right of (1.1). In a leading approximation, which should be adequate at the low frequencies relevant for infrasound, the outer boundary of the wake can be regarded as fixed relative to the moving train, and therefore to form a uniformly convecting boundary (depicted by the wavy lines in Fig. 1) between the vortical interior wake motions and the exterior irrotational unsteady flow. Thus, when the shape of the wake boundary is known its influence on the exterior flow can be accounted for simply by regarding it as a *continuation of the train boundary*. In other words, the combined effects of the train and wake are given by source (1.3) provided $\mathscr{A}_T(x+Ut)$ is taken to define the cross-sectional area of the solid body imagined to be formed by the train and its wake. The simplest such model, discussed later in this paper, is obtained by assuming the wake boundary to consist of a semi-infinite circular cylinder (coaxial with the train) extending downstream from the separation point on the tail of the train. In this case $\partial \mathscr{A}_T/\partial x=0$ in the axial region occupied by the wake, which therefore (see (1.3)) does not generate sound. However, because separation occurs upstream of the end of the train (a distance d_w in Fig. 1), this null source strength actually means that the wake acts to eliminate surface sources that would otherwise be produced by the cross-sectional area variations of the train to the rear of the separation point. The presence of the wake is therefore expected to *reduce* the overall source strength of the tail region.

We shall neglect the small component of the infrasound attributable to the vorticity in the free shear layer of the low-velocity 'jet' flow from the tunnel, produced by the air displaced by the entering train. This is already known (Howe et al., 2000) to have a relatively small influence on the compression wave generated within the tunnel, and its contribution to the exterior sound should be similarly small. The hypothesis is further supported by the results of Section 3 below. Note, however, that observations (Auvity et al., 2001) indicate that vortex roll-up near the mouth can produce a relatively large, slow moving hydrodynamic structure whose *near-field* pressure fluctuations may contribute significantly to pressure measurement made near the mouth.

Each of the separate interactions of the nose and tail with the tunnel entrance occurs typically over a time $\sim R/U$, so that the characteristic wavelength of the infrasound $\sim R/M$ which greatly exceeds the radius h of the train, even at the maximum anticipated train Mach number of $M\sim 0.4$ ($U\approx 500$ kph). Because the mean air flow induced by the train is confined to the immediate neighbourhood of the train, it follows that the convection and scattering of the sound by this flow can be expected to be small. Eq. (1.1) can therefore be approximated by

$$\left(\frac{1}{c_o^2}\frac{\partial^2}{\partial t^2}-\nabla^2\right)B=U\left(1+\frac{\mathscr{A}_o}{\mathscr{A}}\right)\frac{\partial}{\partial t}\left(\frac{\partial \mathscr{A}_T}{\partial x}(x+Ut)\delta(y)\delta(z)\right), \tag{1.4}$$

where here and henceforth $\mathscr{A}_T(x+Ut)$ is to be interpreted as the cross-section of the train and its wake.

This equation is solved in Section 2 in terms of the exact Green's function for a semi-infinite circular cylinder. The infrasound is produced by the interaction of the duct entrance with the near field of the source on the right-hand side. For the case depicted in Fig. 1, and for comparison with the experiments discussed below in Section 4, the circular cylindrical tunnel walls are taken to be rigid, on which the normal derivative $\partial B/\partial x_n=0$. The solution is used in Section 3 to examine the Mach number dependence and the directionality of the infrasound. Approximate formulae are then derived for the prediction of the infrasound produced by a train of arbitrary nose profile, in which the effects of Mach number and the directionality are separated out from those produced by the geometrical shape of the nose and tail of the train. Predictions are compared (Section 4) with track side measurements of the infrasound made by Iida et al. (2001). There is good overall agreement except in radiation directions in front of the tunnel. Here both theory and

experiment indicate relatively weak sound levels. Calculations are performed that suggest that, at least for these experiments, the measured pressures in these directions are dominated by the near-field pressure fluctuations of the passing train.

2. General representation of the infrasound

2.1. Green's function

When the source on the right of Eq. (1.4) is prescribed, the equation can be solved exactly by making use of Green's function $G(\mathbf{x}, \mathbf{x}', t-\tau)$ that has vanishing normal derivative on the inner and outer walls of the semi-infinite, circular cylindrical tunnel walls. $G(\mathbf{x}, \mathbf{x}', t-\tau)$ is the solution of

$$\left(\frac{1}{c_o^2}\frac{\partial^2}{\partial t^2} - \nabla^2\right) G = \delta(\mathbf{x}-\mathbf{x}')\delta(t-\tau), \quad G = 0 \text{ for } t<\tau \tag{2.1}$$

and represents the sound produced by an impulsive point source located $\mathbf{x}'$ at time τ in the presence of the cylinder.

The solution of (2.1) can be cast in the form of a Fourier integral by first writing

$$G(\mathbf{x}, \mathbf{x}', t-\tau) = G_o(\mathbf{x}, \mathbf{x}', t-\tau) + G_s(\mathbf{x}, \mathbf{x}', t-\tau), \tag{2.2}$$

where $G_o(\mathbf{x}, \mathbf{x}', t-\tau)$ is the 'free space' solution, describing the spherically symmetric wave generated by the point source in the absence of the cylinder. Then $G_s(\mathbf{x}, \mathbf{x}', t-\tau)$ may be interpreted as the secondary wave field produced by the diffraction of this spherical wave by the rigid walled cylinder. Noble (1958) has given a detailed discussion of this diffraction problem for arbitrary source position $\mathbf{x}'$, but the solution can be rendered in a greatly simplified form when the ultimate application is to solve Eq. (1.4), in which the source term on the right-hand side is *axisymmetric*, and when the observer at $\mathbf{x}$ is in the acoustic *far field* of the cylinder (i.e. when $|\mathbf{x}| \to \infty$ outside the cylinder). In that case formulae given in Chapter 3 of Noble (1958) supply

$$\begin{aligned} &G_s(\mathbf{x}, \mathbf{x}', t-\tau) \\ &\quad = \frac{\sin\Theta}{16i\pi^3(1+\cos\Theta)|\mathbf{x}|} \\ &\int\int_{-\infty}^{\infty} \frac{\gamma J_1(\kappa_o R\sin\Theta) W_-(k) I_0(\gamma r') e^{i\{kx' - \omega(t-\tau-|\mathbf{x}|/c_o)\}}\, dk\, d\omega}{(k+\kappa_o)(k+\kappa_o\cos\Theta + i0) W(-\kappa_o\cos\Theta) I_1(\gamma R)}, \\ &\quad |\mathbf{x}| \to \infty, \end{aligned} \tag{2.3}$$

where Θ is the angle in Fig. 1 between the x-axis of symmetry and the ray to the observer at x in the far field, the point source is at $\mathbf{x}' = (x', y', z')$ (with $r' = \sqrt{y'^2 + z'^2}$), J_1, $I_{0,1}$ are Bessel functions, and

$$\left.\begin{aligned} &\kappa_o = \omega/c_o, \gamma = \begin{cases} |k^2 - \kappa_o^2|^{\frac{1}{2}}, & |k| > |\kappa_o|, \\ -i\,\mathrm{sgn}(\kappa_o)|\kappa_o^2 - k^2|^{\frac{1}{2}}, & |k| < |\kappa_o|, \end{cases} \\ &W_-(k) = \sqrt{W(k)} \exp\left\{\frac{ik}{\pi}\int_{o.}^{\infty} \frac{\ln[W(K)/W(k)]\, dK}{K^2 - k^2}\right\}, \\ &W(k) = 2I_1(\gamma R) K_1(\gamma R), \end{aligned}\right\} \tag{2.4}$$

where K_1 is a modified Bessel function (Abramowitz and Stegun, 1970). In (2.3) the singularity of the integrand at $k = -\kappa_o$ is avoided by assigning to κ_o (i.e. to ω) a small positive imaginary part that is subsequently allowed to vanish; similarly, the notation 'i0' indicates that the integration contour in the k-plane is required to pass above the pole at $k = -\kappa_o\cos\Theta$.

2.2. The infrasound

Green's function permits the solution of Eq (1.4) to be cast in the form

$$B(x,t) = U\left(1 + \frac{\mathscr{A}_o}{\mathscr{A}}\right)\frac{\partial}{\partial t}\int\int_{-\infty}^{\infty} G(\mathbf{x}, x', 0, 0, t-\tau)\frac{\partial \mathscr{A}_T}{\partial x'}(x' + U\tau)\, dx'\, d\tau, \tag{2.5}$$

where G is given by (2.2). When the observer position $\mathbf{x}$ is in the acoustic far field the contribution from the free space Green's function G_0 can be discarded, since it merely determines the hydrodynamic near field of the uniformly

convecting source distribution that represents the train. The production of propagating sound waves by the interaction of these sources with the tunnel portal is governed by the component G_s of G.

Thus, because $B \approx p/\rho_o$ far from the tunnel, we find

$$p(\mathbf{x},t) \approx \rho_o U\left(1+\frac{\mathscr{A}_o}{\mathscr{A}}\right)\frac{\partial}{\partial t}\int\int_{-\infty}^{\infty} G_s(\mathbf{x},x',0,0,t-\tau)\frac{\partial \mathscr{A}_T}{\partial x'}(x'+U\tau)\mathrm{d}x'\,\mathrm{d}\tau, \quad |\mathbf{x}|\to\infty,$$
$$= \frac{-\rho_o U\sin\Theta}{16\pi^3(1+\cos\Theta)|\mathbf{x}|}\left(1+\frac{\mathscr{A}_o}{\mathscr{A}}\right)\int\int\int\int_{-\infty}^{\infty}\frac{\partial \mathscr{A}_T}{\partial x'}(x'+U\tau)$$
$$\times\frac{\omega\gamma J_1(\kappa_o R\sin\Theta)W_-(k)\mathrm{e}^{\mathrm{i}\{kx'-\omega([t]-\tau)\}}}{(k+\kappa_o)(k+\kappa_o\cos\Theta+\mathrm{i}0)W_-(-\kappa_o\cos\Theta)I_1(\gamma R)}\mathrm{d}k\,\mathrm{d}\omega\,\mathrm{d}x'\,\mathrm{d}\tau, \tag{2.6}$$

where $[t]=t-|\mathbf{x}|/c_o$ is the retarded time. When the integration variable x' is replaced by $x''=x'+U(\tau-[t])$, it can be seen that the integration with respect to τ in (2.6) yields the factor $2\pi\delta(\omega-Uk)$. Hence, we can write

$$p(\mathbf{x},t) \approx \rho_o U^2\frac{\mathscr{A}_o}{\mathscr{A}}\left(1+\frac{\mathscr{A}_o}{\mathscr{A}}\right)\left(1+\frac{\mathscr{A}_o}{\mathscr{A}}\right)\left(\frac{R}{4\pi|\mathbf{x}|}\right)$$
$$\frac{\sin\Theta}{(1+\cos\Theta)(1+M\cos\Theta)}\frac{\sqrt{1-M^2}}{(1-M)}\times\int_{-\infty}^{\infty}\frac{1}{\mathscr{A}_o}\frac{\partial \mathscr{A}_T}{\partial x'}(x'+U[t])F(x',M,\Theta)\,\mathrm{d}x', \quad |\mathbf{x}|\to\infty, \tag{2.7}$$

where

$$F(x',M,\Theta) = -\mathscr{R}e\int_0^{\infty}\frac{J_1(MkR\sin\Theta)W_-(k)\mathrm{e}^{\mathrm{i}kx'}R\,\mathrm{d}k}{W_-(-Mk\cos\Theta)I_1(kR\sqrt{1-M^2})}. \tag{2.8}$$

The functions $W_-(k)$, $W_-(-Mk\cos\Theta)$ in the integrand of (2.8) are to be evaluated using definition (2.4) with $\kappa_o = Mk$.

2.3. Pressure pulse generated by the front of the train: snub nose approximation

To establish an overall picture of the properties of the infrasound we examine first the sound generated as the nose of the train passes into the tunnel, ignoring for the moment the subsequent contributions from the tail and wake of the train. A specific train nose profile defined by the train cross-section area $\mathscr{A}_T(x)$ is discussed in Section 4, when a comparison is made with experiment. However, for the remainder of this section we shall consider the very convenient, but idealized case of a *snub-nosed* train, whose aspect ratio h/L is very large. In the limit $L\to 0$ we have, formally,

$$\frac{1}{\mathscr{A}_o}\frac{\partial \mathscr{A}_T}{\partial x'}(x'+U[t]) = \delta(x'+U[t]). \tag{2.9}$$

Thus, for the purpose of calculating the infrasound, the nose of the train is now equivalent to a point source of constant strength convecting into the tunnel along the axis of symmetry, and Eq. (2.7) becomes

$$\frac{p(\mathbf{x},t)}{\rho_o c_o^2(\mathscr{A}_o/\mathscr{A})\left(1+\mathscr{A}_o/\mathscr{A}\right)\left(R/4\pi|\mathbf{x}|\right)} \approx \frac{\sin\Theta}{(1+\cos\Theta)(1+M\cos\Theta)}\frac{M^2\sqrt{1-M^2}}{1+M}F(-U[t],M,\Theta). \tag{2.10}$$

The right-hand side of this formula is plotted in Fig. 2a as a function of the nondimensional retarded time $U[t]R$ for $\Theta=90^\circ$ and $M=0.1$, 0.2, 0.3 and 0.4. The front of the train (the 'point source') crosses the tunnel entrance plane $x=0$ at time $t=0$. The figure reveals that the interaction with the tunnel begins when the front of the train is about two tunnel radii ahead of the entrance, producing a rarefaction pulse of width $\sim 2R/M$ and duration $\sim 2R/U$, the maximum negative pressure occurring just before entry into the tunnel. The magnitude of this maximum exhibits significant variations with the radiation angle Θ. These are illustrated in Fig. 2b, where the magnitude of the peak negative pressure is depicted as a polar plot for $M=0.2$–0.4. There is a radiation null along the direction $\Theta=0$ directly in front of the tunnel entrance. This occurs for the following reason: the radiation can be ascribed to an acoustic monopole whose strength is determined by the net unsteady airflow through the tunnel portal produced by the entering train, together with a dipole source orientated parallel to the tunnel axis whose amplitude depends on the hydrodynamic force on the air outside the tunnel applied across the entrance plane of the tunnel because of the inertia of the air inside the tunnel (see Howe, 1998a, Section 3.2). Destructive interference of the radiations from these sources produces the null ahead of the tunnel; but the radiations combine in other directions, producing a progressively increasing peak pressure as Θ increases to 180°. These plots indicate that the amplitude of the sound increases rapidly with the Mach number M. This is illustrated in Fig. 3, where the solid circles represent the peak pressure amplitudes calculated from (2.10) when $\Theta=90^\circ$ for Mach numbers ranging from 0.05 to 0.55, revealing a Mach number dependence close to M^3.

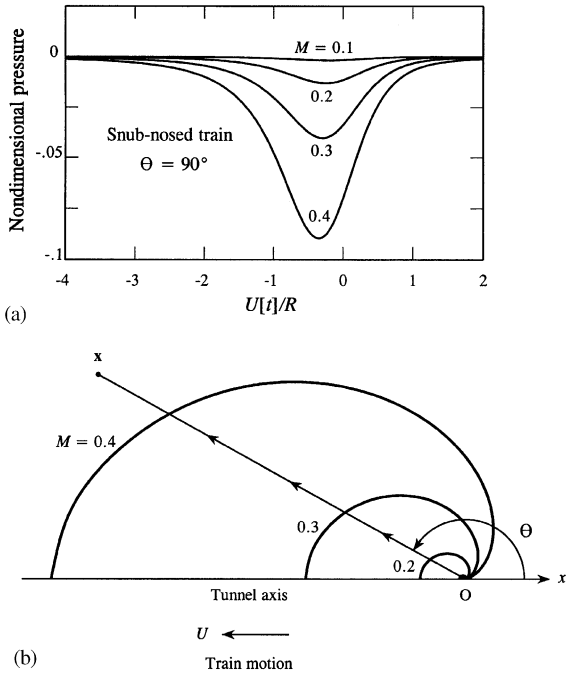

Fig. 2. (a) The nondimensional far-field acoustic pressure signature $p(\mathbf{x},t)/\rho_o c_o^2 \frac{\mathscr{A}_o}{\mathscr{A}}\left(1+\frac{\mathscr{A}_o}{\mathscr{A}}\right)\left(\frac{R}{4\pi|\mathbf{x}|}\right)$ at $\Theta=90^\circ$ produced when the front of a snub-nosed train defined by (2.9) enters the tunnel. (b) Polar plot illustrating the dependence of the peak negative pressure at a fixed radial distance $|\mathbf{x}|$ from the tunnel portal on radiation direction Θ.

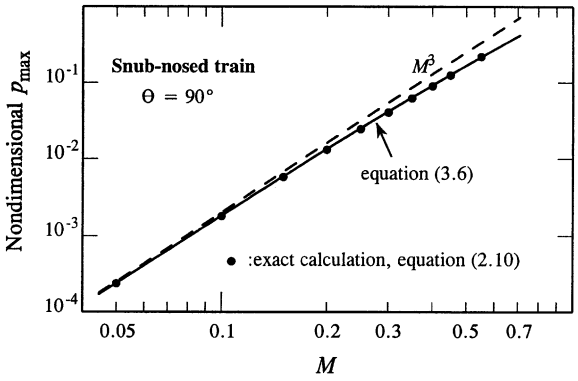

Fig. 3. Dependence on Mach number of the peak absolute pressure at $\Theta=90^\circ$ for a snub nosed train: •, Eq. (2.10); ——, approximation (3.6).

3. Dependence on Mach number and radiation direction

When $M^2 \ll 1$ it follows easily from definitions (2.4) that (for $k>0$)

$$\begin{aligned} J_1(MkR\sin\Theta) &\approx \frac{MkR\sin\Theta}{2}, \quad I_1(kR\sqrt{1-M^2}) \approx I_1(kR) \\ W_-(Mk\cos\Theta) &\approx \mathrm{e}^{\mathrm{i}Mk\ell'\cos\Theta}, \quad \text{where } \ell' = -\frac{R}{\pi}\int_0^\infty \frac{\ln[2I_1(\mu)K_1(\mu)]\mathrm{d}\mu}{\mu^2} \\ W_-(k) &\approx \sqrt{2I_1(kR)K_1(kR)}\exp\left\{\frac{\mathrm{i}k}{\pi}\int_0^\infty \ln\left[\frac{I_1(KR)K_1(KR)}{I_1(kR)K_1(kR)}\right]\frac{\mathrm{d}K}{K^2-k^2}\right\} \end{aligned} \tag{3.1}$$

and therefore that

$$F(x', M, \Theta) \approx \pi R M \sin\Theta \frac{\partial^2 \varphi^*}{\partial x'^2}(x' - M\ell' \cos\Theta, 0, 0), \quad M^2 \ll 1, \tag{3.2}$$

where

$$\frac{\partial^2 \varphi^*}{\partial x'^2}(x', 0, 0) = \frac{-1}{2\pi R}\int_0^\infty \xi\left(\frac{2K_1(\xi)}{I_1(\xi)}\right)^{\frac{1}{2}} \cos\left\{\xi\left(\frac{x'}{R} + \mathscr{Z}(\xi)\right)\right\} \mathrm{d}\xi,$$
$$\mathscr{Z}(\xi) = \frac{1}{\pi}\int_0^\infty \ln\left(\frac{K_1(\mu)I_1(\mu)}{K_1(\xi)I_1(\xi)}\right)\frac{\mathrm{d}\mu}{\mu^2 - \xi^2}. \tag{3.3}$$

To interpret these approximate expressions, observe first that the length $\ell' \approx 0.6127R$ in (3.1) is the acoustic 'end-correction' of the open end of an unflanged cylindrical duct of radius R (Rayleigh, 1926; Noble, 1958). The function $\varphi^*(\mathbf{x})$ is the velocity potential of an ideal, incompressible flow out of the mouth of the duct (at $x = 0$) that satisfies (Howe, 1998c)

$$\varphi^*(\mathbf{x}) \sim \begin{cases} x - \ell' & \text{for } |x| \gg R \text{ inside the duct,} \\ -\mathscr{A}/4\pi|\mathbf{x}| & \text{for } |\mathbf{x}| \gg R \text{ outside the duct,} \end{cases}$$

so that the flow defined by this potential has unit speed at large distances from the mouth inside the duct.

It now follows that, when M^2 is negligible, formula (2.7) for the acoustic pressure can be cast in the form

$$p(\mathbf{x}, t) \approx \frac{\rho_o U^2 M}{4\pi|\mathbf{x}|(1+M)}\left(1 + \frac{\mathscr{A}_o}{\mathscr{A}}\right)\frac{(1-\cos\Theta)}{(1+M\cos\Theta)}\int_{-\infty}^{\infty}\frac{\partial \mathscr{A}_T}{\partial x'}(x' + U[t'])\frac{\partial^2 \varphi^*}{\partial x'^2}(x', 0, 0)\mathrm{d}x',$$
$$M^2 \ll 1, \quad |\mathbf{x}| \to \infty, \tag{3.4}$$

in which the modified retarded time is given by

$$[t'] = t - \frac{(|\mathbf{x}| - \ell'\cos\Theta)}{c_o} \approx t - \frac{|\mathbf{x} - \ell'\mathbf{i}|}{c_o}, \quad |\mathbf{x}| \gg R, \tag{3.5}$$

where $\mathbf{i}$ is a unit vector in the x-direction. Representation (3.4) is a generalization of the approximation derived by Howe (2001, Eq. (4.15)) (based on the theory of compact Green's functions), where the terms in M in the denominators are absent and $[t']$ is replaced by $[t]$.

Approximation (3.4) is of value because it identifies the dependence of the sound on tunnel portal geometry (which governs the functional form of $\varphi^*(\mathbf{x})$), and on the Mach number M and radiation direction Θ. For the snub nosed train defined by the uniformly translating point source (2.9), it yields

$$\frac{p(\mathbf{x}, t)}{\rho_o c_o^2 (1 + \mathscr{A}_o/\mathscr{A})(R/4\pi|\mathbf{x}|)} \approx \frac{\pi M^3 (1 - \cos\Theta)}{(1+M)(1+M\cos\Theta)} R\frac{\partial^2 \varphi^*}{\partial x'^2}(-U([t] + \ell'\cos\Theta/c_o), 0, 0). \tag{3.6}$$

The nondimensional function $R\partial^2\varphi^*(x, 0, 0)/\partial x^2$, evaluated on the axis of symmetry of the tunnel, vanishes except near the tunnel mouth, where it exhibits a deep negative minimum of the type shown in Fig. 2a for $M = 0.4$ (with x identified with $-U[t]/R$); it attains a minimum value of $R(\partial^2\varphi^*/\partial x^2)_{\min} \approx -0.64$ at $x = 0.2R$, just outside the tunnel. The solid curve in Fig. 3 is the nondimensional absolute pressure determined by (3.6) at $\Theta = 90^\circ$ when $R\partial^2\varphi^*/\partial x'^2$ is assigned this minimum value, i.e. it corresponds to the low Mach number approximation to the peak pressure radiated in this direction. It is in excellent agreement with the exact numerical predictions (represented by the solid circles) for Mach numbers M as large as 0.55, much larger than might be expected from our requirement above that $M^2 \ll 1$.

The solid and broken-line directivity curves in Fig. 4 are calculated respectively from Eq. (2.10) and the low Mach number approximation (3.6). Although the agreement is good at $\Theta = 90^\circ$ and for all angles when $M < 0.3$, at larger intermediate angles the approximate formula tends to overpredict the amplitude when $M > 0.3$. The dotted curves are plotted from the following empirical correction to (3.6):

$$\frac{p(\mathbf{x}, t)}{\rho_o c_o^2 (1 + \mathscr{A}_o/\mathscr{A})(R/4\pi|\mathbf{x}|)} \approx \frac{\pi M^3 (1 - \cos\Theta)(1 + 0.4M^2\sin 2\Theta)}{(1+M)(1+M\cos\Theta)} R\frac{\partial^2 \varphi^*}{\partial x'^2}(-U([t] + \ell'\cos\Theta/c_o), 0, 0). \tag{3.7}$$

In Fig. 5 we compare for $M = 0.4$ (the largest value likely to be encountered in applications) the far-field pressure signatures predicted by the exact formula (2.10) (the solid curves) and approximation (3.7) (dotted) for the snub-nosed

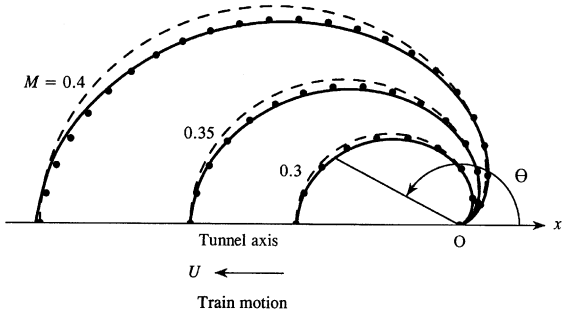

Fig. 4. The exact directivity of the peak pressure amplitude (——) determined by Eq. (2.10) for a snub-nosed train compared with approximation (3.6) (- - - -) and the corrected approximation (3.7) (• • •).

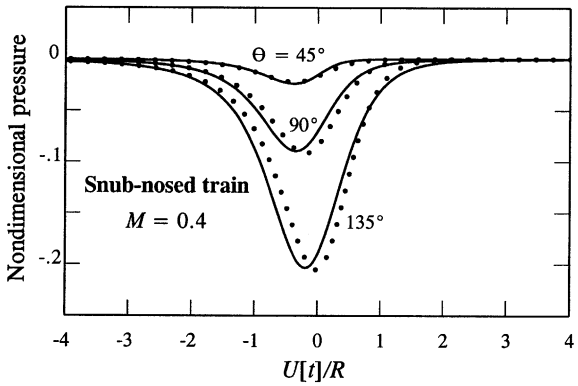

Fig. 5. Nondimensional far-field acoustic pressure signature $p(\mathbf{x},t)/\rho_o c_o^2 \frac{\mathscr{A}_o}{\mathscr{A}}\left(1+\frac{\mathscr{A}_o}{\mathscr{A}}\right)\left(\frac{R}{4\pi|\mathbf{x}|}\right)$ at $\Theta=45^\circ$, 90°, 135° produced when the front of the snub-nosed train (2.9) enters the tunnel at $M=0.4$: ——, exact formula (2.10); • • •, approximation (3.7).

train for $\Theta=45^\circ$, 90° and 135°. The predictions are essentially the same, except for small differences in *phase* that are unimportant in practice.

These results suggests that a uniform approximation for $M\leqslant 0.4$ and arbitrary train nose profile is supplied by the following modification of (3.4):

$$p(\mathbf{x},t)\approx\frac{\rho_o U^2 M}{4\pi|\mathbf{x}|(1+M)}\left(1+\frac{\mathscr{A}_o}{\mathscr{A}}\right)\frac{(1-\cos\Theta)(1+0.4M^2\sin 2\Theta)}{(1+M\cos\Theta)}\times\int_{-\infty}^{\infty}\frac{\partial\mathscr{A}_T}{\partial x'}(x'+U[t'])\frac{\partial^2\varphi^*}{\partial x'^2}(x'0,0)\,\mathrm{d}x',\quad |\mathbf{x}|\to\infty. \tag{3.8}$$

It is interesting to note that the integral in this formula is identical with that determining the 'gradient' of the wavefront of the compression wave radiated into the tunnel ahead of the train. This can be taken to justify our neglect of the exit flow vorticity in the calculation of the infrasound, since it would occur here in exactly the same relative terms as in the compression wave problem, where its contribution is known to be small (Howe et al., 2000).

The infrasound and the compression wave in the tunnel are generated simultaneously. The latter emerges from the far end of the tunnel as the 'micro-pressure' wave whose peak amplitude scales approximately as M^3, the same as illustrated in Fig. 3 for the peak infrasound. We can, in fact, interpret the micro-pressure wave as another manifestation of the infrasound that radiates into the open air only after being modified (by wave steepening or damping, depending on track conditions) during its propagation along the length of the tunnel.

4. Comparison with experiment

4.1. Experiments of Iida et al. (2001)

The model scale experiments of Iida et al. (2001) outlined in Section 1 involved a train with ellipsoidal nose and tail sections. The nose profile is obtained by rotating the curve $y = h\sqrt{(x/L)(2-x/L)}, 0<x<L$ about the x-axis; the overall cross-sectional area distribution of the train is therefore given by

$$\frac{\mathscr{A}_T(s)}{\mathscr{A}_o} = \begin{cases} \frac{s}{L}(2-\frac{s}{L}) & 0<s<L, \\ 1, & L<s<\ell-L, \\ (\frac{\ell}{L}-\frac{s}{L})(2-\frac{\ell}{L}+\frac{s}{L}), & \ell-L<s<\ell. \end{cases} \tag{4.1}$$

where (see Fig. 1)

$$h = 2.235\,\text{cm}, \quad L = 6.7\,\text{cm}, \quad \ell = 59.3\,\text{cm}.$$

The tunnel radius $R=5$ cm, and the blockage $\mathscr{A}/\mathscr{A}_o \approx 0.2$.

To calculate the sound the wake is assumed to have a circular cylindrical mean boundary, and to separate from the train at a distance d_w ahead of the tip of the tail. Then the effective 'source' strength $\partial\mathscr{A}_T(s)/\partial x'$ in the exact and approximate solutions (2.7) and (3.8) is nonzero only in the interval $0<s<\ell-d_w$, where

$$\frac{1}{\mathscr{A}_o}\frac{\partial\mathscr{A}_T}{\partial x'}(s) = \begin{cases} \frac{2}{L}(1-\frac{s}{L}), & 0<s<L, \\ 0, & L<s<\ell-L, \\ \frac{2}{L}(\frac{\ell}{L}-1+\frac{s}{L}), & \ell-L<s<\ell-d_w. \end{cases} \tag{4.2}$$

The acoustic pressure was measured at a constant offset distance of $10R$ from the axis of symmetry of the tunnel, at the three stations (i), (ii), (iii) indicated in Fig. 6, corresponding respectively to $(|\mathbf{x}|,\Theta) = (10\sqrt{2}R, 45^\circ), (10R, 90^\circ), (10\sqrt{2}R, 135^\circ)$.

The open triangles in Fig. 7 and 8 represent the measured acoustic pressures plotted as a function of $U[t]R$, respectively, for train speeds $U=409$ and 251 kph ($M\approx 0.33$, 0.2). The nose of the train crosses the plane $x=0$ of the tunnel entrance at $U[t]/R=0$, and the train is fully within the tunnel when $U[t]/R>\ell/R\approx 11.9$. At these times the measurements at stations (ii) and (iii) exhibit large negative and positive peaks as the train nose and tail pass into the tunnel: the negative pulse of duration $\sim 2R/U$ is generated by the nose interacting with the tunnel entrance. The positive pressure peak produced by the tail of the train (at $U[t]/R\sim 11$) is similar in structure but smaller in amplitude. The time histories of the pressures received at station (i) are similar for the two different train speeds, but no clear peaks are evident. Iida et al. (2000, 2001) conjectured that the relatively weak radiation at this station is overwhelmed by the near field (nonacoustic, or 'pseudo-sound') pressure fluctuations generated by the passing train.

The solid and dotted curves in Figs. 7 and 8 are the predictions of the exact and approximate solutions (2.7) and (3.8), respectively. The differences between these predictions are negligible; even the phase differences noted previously in Fig. 5 at higher Mach numbers are of no practical significance. In the calculations we have assumed that the wake separates from the tail at a distance $d_w=0.2L$ from the tip of the tail; there is no theoretical or observational justification for this assumption, but it is consistent with numerical predictions reported by Schetz (2001). The corresponding agreement with experiment is seen to be good at station (iii) at both train speeds, with excellent predictions of both peaks. Note that the wake acts to reduce the amplitude of the second peak; if the wake were ignored it would hardly alter predictions at station (ii) relative to experiment, but there would be poor agreement of the predicted and measured second peaks at station (iii). The theory fails to capture the uniformly negative pressures recorded at stations (ii) and (iii) in the interval $2<U[t]/R<10$, and the overall agreement is much worse at station (ii). At station (i), in front of the tunnel, the predictions can arguably be associated with small excursions of the observed pressure profiles, but are very weak and appear to be submerged within the near field noise conjectured by Iida et al. (2000, 2001).

4.2. Influence of near field pressure fluctuations

A proper estimate of the contribution to the measured pressures at stations (i)–(iii) of the 'hydrodynamic' pressure fluctuations produced by the passing train and by its entrance into the tunnel can be made provided the appropriate functional form of Green's function (2.2) is known. Approximation (2.3) is applicable only in the 'acoustic far field', where the hydrodynamic effects are supposedly negligible. Formulae given in Noble (1958) are in principle sufficient to

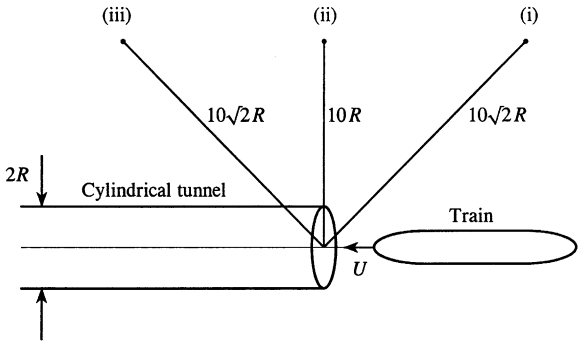

Fig. 6. Acoustic pressure measurement stations (i), (ii), (iii), respectively, at $(|\mathbf{x}|, \Theta) = (10\sqrt{2}R, 45°), (10R, 90°), (10\sqrt{2}R, 135°)$.

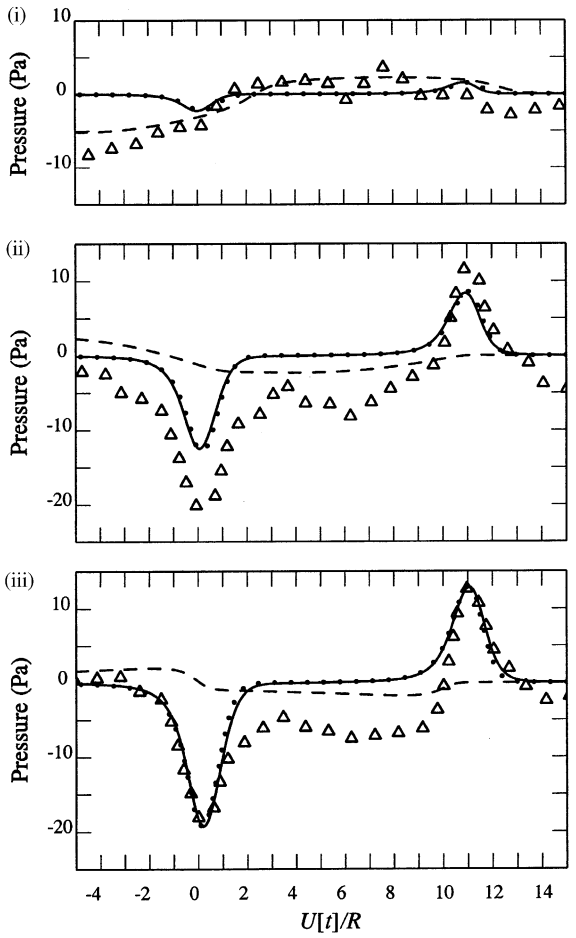

Fig. 7. △ △ △, measured pressures at Stations (i)–(iii) for $U = 409$ kph; ——, infrasound prediction of the exact solution (2.7); ● ● ●, the approximation (3.8); - - - -, near-field approximation (4.9).

determine $G(\mathbf{x}, \mathbf{x}', t-\tau)$ everywhere, but they are difficult to apply except with the assistance of extensive numerical computations.

However, a straightforward approximation to both the acoustic near and far fields can be made in explicit analytic form by using the 'compact' approximation to $G(\mathbf{x}, \mathbf{x}', t-\tau)$, which is applicable when the characteristic wavelength of

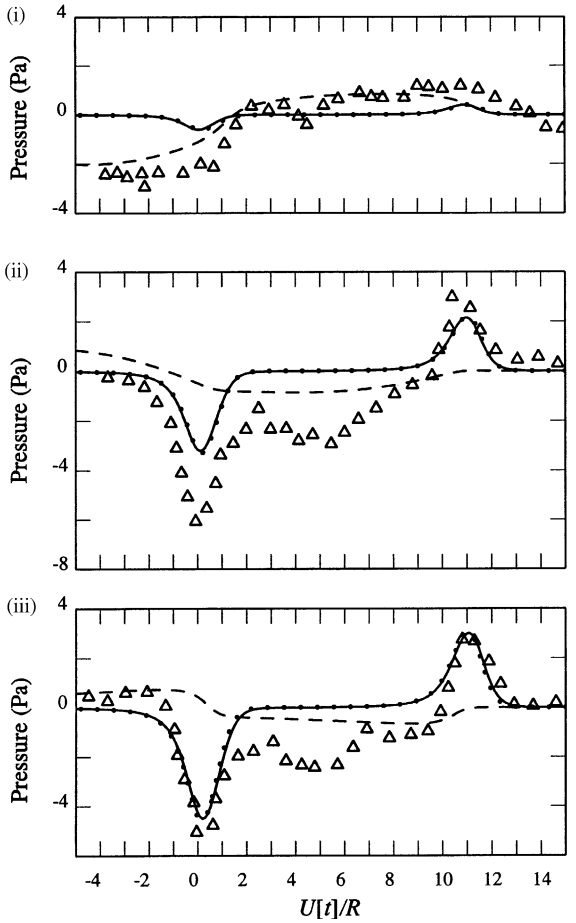

Fig. 8. △ △ △, measured pressures at Stations (i)–(iii) for $U=251$ kph; ——, infrasound prediction of the exact solution (2.7); • • •, approximation (3.8); - - - -, near-field approximation (4.9).

the sound is known to be large compared to the duct radius R. It is given by (Howe, 1998a)

$$G(\mathbf{x},\mathbf{x}',t-\tau)=\frac{1}{4\pi|\mathbf{X}-\mathbf{X}'|}\delta\left(t-\tau-\frac{(|\mathbf{X}-\mathbf{X}'|-[\varphi^*(\mathbf{x})+\varphi^*(\mathbf{x}')])}{c_o}\right), \tag{4.3}$$

provided either the source position $\mathbf{x}'$ or observer position $\mathbf{x}$ is located at a large distance ($\gg R$) from the duct entrance in *free space*. The function φ^* is defined as in Section 3.1; $\mathbf{X}=(X(\mathbf{x}),Y(\mathbf{x}),Z(\mathbf{x}))$ is called the Kirchhoff vector for the duct entrance, and is defined such that its component in the i-direction is equal to the velocity potential of incompressible flow from infinity *outside* the duct that has unit speed in the i-direction at large distances from the entrance (and is exponentially small at large distance $|x|$ *within* the tunnel), i.e.

$$\mathbf{X}\sim\begin{cases}\mathbf{x},\ |\mathbf{x}|\to\infty \text{ outside the duct},\\ 0,\ x\to\infty \text{ inside the duct}.\end{cases}$$

$\mathbf{X}$ can be evaluated in analytic form for a circular cylindrical duct. In particular $X\equiv x-\varphi^*(\mathbf{x})$, so that $\mathbf{X}\equiv(x-\varphi^*(\mathbf{x}),Y(\mathbf{x}),Z(\mathbf{x}))$ and $\mathbf{X}'\equiv(x'-\varphi^*(\mathbf{x}'),Y(\mathbf{x}'),Z(\mathbf{x}'))$.

The representation (4.3) is an approximate solution of the Green's function Eq. (2.1) that agrees with the exact Green's function when the latter is expanded in a multipole series in which all terms of quadrupole order and higher are discarded. When the Mach number $M=U/c_o$ is small the wavelength of the infrasound generated when the train enters the tunnel $\sim O(R/M)\gg R$, and this limiting case was examined by Howe (2001) using (4.3). The procedure yields the

following low Mach number limit of the acoustic far field (3.8):

$$p(\mathbf{x},t)\approx\frac{\rho_o U^2 M}{4\pi|\mathbf{x}|}\left(1+\frac{\mathscr{A}_o}{\mathscr{A}}\right)(1-\cos\Theta)\int_{-\infty}^{\infty}\frac{\partial\mathscr{A}_T}{\partial x'}(x'+U[t'])\frac{\partial^2\varphi^*}{\partial x'^2}(x',0,0)\mathrm{d}x',\quad |\mathbf{x}|\to\infty. \tag{4.4}$$

However, (4.3) can also be used to determine the hydrodynamic component of the far field. To do this we first observe that the characteristic frequency of the near-field pressure decreases with distance from the train like U/r, where r denotes lateral distance from the axis of the tunnel. These pressures accordingly make a relatively low-frequency contribution to the 'sound' at the measurement points, where $r=10R$, and cannot be significantly dependent on the shapes of the train nose and tail. For the purpose of estimating the near-field contribution to the pressure it is therefore sufficient to ignore the detailed geometries of the train nose and tail, and to use of the following approximation for $\mathscr{A}'_T$:

$$\frac{1}{\mathscr{A}_o}\frac{\partial\mathscr{A}_T}{\partial x'}(x'+U\tau)=\delta(x'+\ell_c+U\tau)-(1-\Delta)\delta(x'-\ell+\ell_c+U\tau), \tag{4.5}$$

where $\ell_c=\frac{2}{3}L$ is the distance of the *centroid* of the nose monopole distribution from the nose tip, and the term

$$\Delta=\frac{d_w}{L}\left(2-\frac{d_w}{L}\right) \tag{4.6}$$

accounts for the reduction in the negative source strength of the tail produced by the wake. This source is to be used in (2.5). Near-field pressure fluctuations produced by the motion of sources (4.5) prior to the arrival at the tunnel entrance are uninfluenced by the pressure drag on the nose of the train arising as the train enters the tunnel. At such times the factor $\mathscr{A}_o/\mathscr{A}$ in (2.5), which takes formal account of the drag dipole, should therefore be omitted. Because our theory does not include a smooth transition between the absence and presence of this dipole, and because the correction produced by the factor $\mathscr{A}_o/\mathscr{A}$ is in our case only 20%, we shall omit this term for all times. Indeed (see below), there is a rapid cut-off of near-field contributions from a source once it has entered the tunnel, so that the approximation is unlikely to have a significant influence on our predictions.

At the relatively low frequencies that characterize the near field of the train, the pressure field is convected along steadily by the moving train prior to being cut-off by tunnel entry, and possible changes occurring during the time required for the passage of an acoustic disturbance from the tunnel mouth to the observer can be ignored. Thus, the near-field approximation of Green's function (4.3) may be taken in the form

$$G(\mathbf{x},\mathbf{x}',t-\tau)\approx\frac{1}{4\pi|\mathbf{x}-\mathbf{X}'|}\delta(t-\tau), \tag{4.7}$$

and used to evaluate (2.5) with the omission of the factor $(1+\mathscr{A}_o/\mathscr{A})$. At the measurement stations (i)–(iii) the unsteady motion is irrotational with velocity potential $\phi(\mathbf{x},t)$, say, and (2.5) determines $\phi(\mathbf{x},t)$ from the relation

$$-\frac{\partial\phi}{\partial t}\equiv B\approx\frac{p}{\rho_o}+\frac{1}{2}(\nabla\phi)^2, \tag{4.8}$$

where, after integrating with respect to time, Eq. (2.5) and (4.7) imply that the hydrodynamic near field is given by

$$\phi(\mathbf{x},t)\approx\frac{U}{4\pi}\int_{-\infty}^{\infty}\frac{\mathscr{A}'_T(x'+Ut)\mathrm{d}x'}{|\mathbf{x}-\mathbf{i}X(x',0,0)|}, \tag{4.9}$$

where $\mathbf{i}$ is a unit vector in the x-direction. It follows from this and Eq. (4.5) that at the observation points (i)–(iii) the terms on the right of (4.8) have the relative magnitudes

$$(\nabla\phi)^2\sim\left(\frac{R}{r}\right)^2\frac{p}{\rho_o}\ll\frac{p}{\rho_o},$$

and therefore that the near-field pressure $p\approx\rho_o B$, as in the acoustic field, so that

$$\begin{aligned}p(\mathbf{x},t)&\approx\frac{-\rho_o U^2}{4\pi}\int_{\infty}^{\infty}\frac{\partial}{\partial x'}\left(\frac{1}{|\mathbf{x}-\mathbf{i}X(x',0,0)|}\right)\mathscr{A}'_T(x'+Ut)\,\mathrm{d}x'\\&=\frac{-\rho_o U^2\mathscr{A}'_o}{4\quad\mathscr{A}}(\mathscr{F}(\mathbf{x},-Ut+\ell_c,0,0)-(1-\Delta)\mathscr{F}(\mathbf{x},-Ut+\ell_c,0,0)),\end{aligned} \tag{4.10}$$

where

$$\mathscr{F}(\mathbf{x},\mathbf{x}')\equiv\frac{\partial}{\partial x'}\left(\frac{R^2}{|\mathbf{x}-\mathbf{i}X(\mathbf{x}')|}\right)=\frac{R^2(x-x'+\varphi^*(\mathbf{x}'))}{|\mathbf{x}-\mathbf{i}(x'-\varphi^*(\mathbf{x}'))|^3}\left(1-\frac{\partial\varphi^*}{\partial x'}(\mathbf{x}')\right). \tag{4.11}$$

The formula (Howe, 1998c)

$$\frac{\partial\varphi^*}{\partial x'}(x',0,0)=\frac{1}{2}-\frac{1}{2\pi}\int_{-\infty}^{\infty}\left(\frac{2K_1(\xi)}{I_1(\xi)}\right)^{1/2}\sin\left\{\xi\left(\frac{x'}{R}+\mathscr{Y}(\xi)\right)\right\}\mathrm{d}\xi \tag{4.12}$$

can be used to evaluate the function $\mathscr{F}(\mathbf{x},\mathbf{x}')$ of (4.11), where $\mathscr{Y}(\xi)$ is defined as in (3.3). But (4.12) implies that $1-\partial\varphi^*(\mathbf{x}')/\partial x'$ is exponentially small within the tunnel. Therefore, because $\varphi^*(\mathbf{x}')$ is small outside the tunnel and near the tunnel entrance, we can approximate $\mathscr{F}(\mathbf{x},\mathbf{x}')$ by

$$\mathscr{F}(\mathbf{x},\mathbf{x}')\approx\frac{R^2(x-x')}{|\mathbf{x}-\mathbf{i}x'|^3}\left(1-\frac{\partial\varphi^*}{\partial x'}(\mathbf{x}')\right).$$

This function characterizes the spatial variations of the near field of the train outside the tunnel; it tends smoothly to zero as the source point $\mathbf{x}'$ passes into the tunnel, which then 'shields' it from an exterior observer.

The calculated contributions from the near field correction are plotted as the broken line curves in Figs. 7 and 8. The time t and $[t]$ are effectively identical for the near-field pressure, which hardly varies during the time required for a pressure pulse to travel from the tunnel exit to the observation point. The results for both Mach numbers at station (i) indicate that the near-field pressures actually dominate the measured pressure fluctuations. Elsewhere the near-field corrections yield overall pressure variations that are qualitatively consistent with the extended negative pressures observed in the interval $2<U[t]/R<10$, but are too small to account fully for the experimental results. It is possible that the additional pressures are associated with the near field of the large torroidal vortex observed to be ejected from the tunnel mouth as the front of the train enters the tunnel (Auvity et al., 2001). This vortex also generates infrasound by interaction with the tunnel mouth, but only as the train nose enters the tunnel, when the additional relative acoustic pressure fluctuations are expected to be similar in magnitude to those occurring during compression wave formation in the tunnel, viz about 5% (cf. Our remark above following Eq. (3.8)). However, more detailed observations are necessary in order to decide whether the large differences between theory and experiment evident in Figs. 7 and 8 are a consequence of the measurement technique or are caused by these additional hydrodynamic aspects of the entry flow.

5. Conclusion

The mean pressure $p_o(t)$, say, just ahead of a train rises as the train approaches a tunnel portal. The pressure rise propagates into the tunnel forming a compression wave whose wavefront thickness is proportional to the time required for the nose of the train to pass into the tunnel. The production of this wave creates a transient flow of air through the tunnel mouth of mass flux $\sim\mathscr{A}p_o(t)/c_o$. This flux is acoustically equivalent to a low-frequency monopole sound source that radiates (in the 'free space') outside the tunnel with an essentially uniform directivity. In addition, however, a net force $\alpha\mathscr{A}p_o(t)$ is exerted on the air outside the tunnel, over the tunnel entrance cross-section and over the solid area of the exterior tunnel portal, where the 'efficiency factor' α is a function $\mathscr{A}/\mathscr{A}_E$, $\mathscr{A}_E$ being the tunnel cross-sectional area $\mathscr{A}$ augmented by the solid face area of the portal. This force constitutes an acoustic dipole, so that the *net* infrasound radiation from the portal at low Mach numbers is proportional to

$$\frac{(\alpha\cos\Theta-1)\mathscr{A}}{c_o|\mathbf{x}|}\frac{\partial p_o}{\partial t}\left(t-\frac{|\mathbf{x}|}{c_o}\right). \tag{5.1}$$

The theory and experiments discussed in this paper are concerned with the infrasound generated at a 'hood-like' tunnel entrance, modeled by the end of a long circular cylindrical, thin walled duct (so that $\mathscr{A}_E\equiv\mathscr{A}$). Our analysis using the exact acoustic Green's function for the special case of an axisymmetric train entering along the axis of the tunnel confirms that $\alpha=1$ in this case, and also permits predictions to be made at the higher Mach numbers (~0.4) of newer trains. Predictions are in general agreement with measurement (Iida et al., 2001), but both experiment and theory imply that in practice it may also be important to include contributions from the near-field ('pseudo-sound') pressure fluctuations generated by the train when making estimates of the overall intensity of the infrasound impinging on dwellings and other structures close to the tunnel portal.

Eq. (5.1) suggests for more general tunnel entrance geometries that the directionality of the infrasound depends critically on the value of α. Preliminary calculations not reported here indicate that $\alpha<1$ when $\mathscr{A}_E>\mathscr{A}$ for 'flanged' tunnels of circular cross-section, and that the dipole strength progressively decreases with increasing flange size, ultimately decaying like $(\mathscr{A}/\mathscr{A}_E)^{1/2}$. Similarly, the relative configuration of the train and tunnel will usually be *asymmetric*, and in practice it will also be important to include estimates of the dipole sound generated by the resulting 'side-force' exerted on the air when the train enters the tunnel. This dipole is orientated parallel to any tunnel flange,

and its contribution to the infrasound will therefore be effectively independent of $\mathscr{A}_E$. It may be calculated in a first approximation by the methods of this paper using the compact Green's function (4.3).

References

Abramowitz, M., Stegun, I.A. (Eds.), 1970. Handbook of Mathematical Functions (Ninth corrected printing), US Department of Commerce, National Bureau of Standards Applied Mathematics Series No. 55, Washington D.C.

Auvity, B., Bellenoue, M., Kageyama, T., 2001. Experimental study of the unsteady aerodynamic field outside a tunnel during train entry. Experiments in Fluids 30, 221–228.

Fox, J.A., Vardy, A.E., 1973. The generation and alleviation of air pressure transients caused by the high speed passage of vehicles through tunnels. Paper G3, BHRA Symposium of the Aerodynamics and Ventilation of Vehicle Tunnels, University of Kent, England, pp. 49–64.

Hara, T., Kawaguti, M., Fukuchi, G., Yamamoto, A., 1968. Aerodynamics of high-speed train. Monthly Bulletin of the International Railway Congress Association XLV (2), 121–146.

Howe, M.S., 1998a. Acoustics of Fluid-Structure Interactions, Cambridge University Press, Cambridge.

Howe, M.S., 1998b. Mach number dependence of the compression wave generated by a high-speed train entering a tunnel. Journal of Sound and Vibration 212, 23–36.

Howe, M.S., 1998c. The compression wave produced by a high-speed train entering a tunnel. Proceedings of the Royal Society A 454, 1523–1534.

Howe, M.S., 1999. On the compression wave generated when a high-speed train enters. a tunnel with a flared portal. Journal of Fluids and Structures 13, 481–498.

Howe, M.S., Iida, M., Fukuda, T., Maeda, T., 2000. Theoretical and experimental investigation of the compression wave generated by a train entering a tunnel with a flared portal. Journal of Fluid Mechanics 425, 111–132.

Howe, M.S., 2001. Vorticity and the theory of aerodynamic sound. Third Lighthill Memorial Paper: Journal of Engineering Mathematics 41, 367–400.

Iida, M., Kikuchi, K., Fukuda, T. 2000. A pressure wave radiated from a tunnel entrance when a train enters a tunnel. Paper presented at the 10th International Symposium on Aerodynamics and Ventilation of Vehicle Tunnels, Boston, USA.

Iida, M., Y. Tanaka, K. Kikuchi, Fukuda, T., 2001. Characteristics of the pressure wave radiated from an entrance portal when a train enters at tunnel. Proceedings of the 50th Japan National Congress on Theoretical and Applied Mechanics, Tokyo.

Nobel, B., 1958. Methods Based on the Wiener–Hopf Technique. Pergamon Press, London. (Reprinted 1988, Chelsea Publications, New York).

Ozawa, S., Tsukamoto, K., Maeda, T., 1976. Model experiments on devices to reduce pressure wave radiated from a tunnel (in Japanese). Railway Technical Research Institute, Japanese National Railways, Rept. No. 990.

Ozawa, S., Maeda, T., 1988. Model experiment on reduction of micro-pressure wave radiated from tunnel exit. Proceedings of the International Symposium on Scale Modeling, Japan Society of Mechanical Engineers, Tokyo, Japan.

Ozawa, S., Maeda, Matsumura, T., Uchida, K., Kajiyama, H., Tanemoto, K., 1991. Countermeasures to reduce micro-pressure waves radiating from exits of Shinkansen tunnels. Aerodynamics and Ventilation of Vehicle Tunnels, Elsevier Science Publishers, Amsterdam, pp. 253–266.

Rayleigh, L., 1926. The Theory of Sound, Vol. 2. Macmillan, London.

Schetz, J.A., 2001. Aerodynamics of high-speed trains. Annual Reviews of Fluid Mechanics 33, 371–414.

Woods, W.A., Pope, C.W., 1976. Secondary aerodynamic effects in rail tunnels during vehicle entry. Paper C5, Second BHRA Symposium of the Aerodynamics and Ventilation of Vehicle Tunnels, Cambridge, England, pp. 71–86.

Yoon, T., Lee, S., 2001. Efficient prediction methods for the micro-pressure wave from a high-speed train entering a tunnel using the Kirchhoff formulation. Journal of the Acoustical Society of America 110, 2379–2389.